49th AIAA Aerospace Sciences Meeting including the New Horizons Forum and Aerospace Exposition
4 - 7 January 2011, Orlando, Florida

AIAA 2011-138

Interactions of Single-Nozzle Supersonic Propulsive Deceleration Jets on Mars Entry Aeroshells

Hicham Alkandry* and Iain D. Boyd†

Department of Aerospace Engineering, University of Michigan, Ann Arbor, MI, 48109

Erin M. Reed‡, Joshua R. Codoni§, and James C. McDaniel¶

Department of Mechanical and Aerospace Engineering, University of Virginia, Charlottesville, VA, 22903

The effects of the propulsive decelerator (PD) jet Mach number on the flowfield, surface, and aerodynamic properties of a Mars entry aeroshell are investigated in Mach 12 laminar flow of I_2-seeded N_2 gas. This is achieved using the computational fluid dynamics (CFD) code LeMANS, as well as the planar laser-induced iodine fluorescence (PLIIF) experimental technique. The results show that the flowfield features, such as the standoff distance of the bow and jet shocks, are all affected by the PD jet Mach number. The results also show that as the thrust coefficient increases, the flow around the aeroshell approaches a jet-only, no freestream configuration due to a PD jet shield. Therefore, the effects of the PD jet Mach number on the surface properties and the drag coefficient increases. As a result, the difference in the drag coefficient between the supersonic and sonic jets increases to as much as 25%. However, since the drag is inversely proportional to the nozzle thrust, the total axial forces for the supersonic and sonic jets are in close agreement, with a maximum difference of 4%. This result indicates that the overall deceleration performance of the aeroshell is only slightly affected by the PD jet Mach number for these particular conditions. The study also shows that propulsive deceleration with central PD jets may only be beneficial for thrust coefficients greater than 1.5 for both sonic and supersonic jets; a result that appears to be independent of the jet exit Mach number. Finally, qualitative comparisons between LeMANS and PLIIF show overall good agreement in the bow shock profile and standoff distance.

Nomenclature

C_D	Drag Coefficient
C_f	Coefficient of Skin Friction
C_P	Pressure Coefficient
C_T	Thrust Coefficient
F_D	Drag Force [N]
Kn	Knudsen Number
M	Mach Number
$\dot{m}$	Mass Flow Rate [kg/s]
P	Pressure [Pa]
Re	Reynolds Number
S	Aeroshell Frontal Area [m^2]
U	Velocity [m/s]
X	Mole Fraction
γ	Ratio of Specific Heats

*Graduate Student, Student Member AIAA.
†Professor, Associate Fellow AIAA.
‡Graduate Student, Student Member AIAA.
§Graduate Student, Student Member AIAA.
¶Professor, Associate Fellow AIAA.

ρ Density [kg/m^3]
τ Shear Stress [Pa]

subscripts
0 Total (Stagnation) Conditions
jet PD Jet Conditions
ref Reference Freestream Conditions

I. Introduction

ALTERNATIVE entry, descent, and landing (EDL) technologies are needed for future high-mass Mars entry systems due to mass and size limitations of the current conventional aerodynamic decelerators.[1] The Mars Science Laboratory (MSL) spacecraft, scheduled for launch in the Fall of 2011, has an estimated landing mass larger than 1700 kg, which is far greater than the entry mass for any previous Mars entry system (e.g. Viking).[2] The MSL will also land at a site that is up to 1 km above the reference altitude. Future missions, including possible human exploration missions, may continue this trend of carrying more payload masses to Mars in order to conduct more sophisticated *in situ* experiments and landing at sites of scientific interest that are at higher altitudes. However, it may not be possible to simply extend the Viking-heritage technology (e.g. supersonic Disk-Gap-Band parachutes and 70° blunt body aeroshells) to the dimensions and deployment conditions required by these missions.[1] One promising approach to resolve these challenges is to use an additional propulsive decelerator (PD) component in order to slow the vehicle down to appropriate speeds by directing engine thrust into the incoming freestream.

Previous work on PD jets began in the 1960s and early 1970s. This work mainly examined the aerodynamic effects through wind tunnel experiments of supersonic PD jets fired into an incoming supersonic freestream. Experimental results showed that for relatively low non-dimensional nozzle thrust values, only a small augmentation of the axial force (the sum of the aerodynamic drag and the thrust forces) beyond that provided by the PD jet off case was observed for the single-nozzle configuration.[3] From the 1970s until the present, however, there has not been any significant work on propulsive deceleration. Today, several different EDL architectures for human-scale Mars missions are being considered,[4] which include an all-propulsive design with PD jets firing into an incoming hypersonic freestream. This architecture, however, involves complex flow interactions that are still not well understood due to several important limitations. These limitations include a lack of extensive experimental data and validated numerical approaches that can accurately and efficiently simulate the complex flow interactions that are generated in the use of these PD jets in a hypersonic freestream.

This paper will describe numerical and experimental approaches that are used to understand the complex flow interactions between the PD jets, a hypersonic freestream, and the aeroshell. It will also present numerical results using a scaled MSL aeroshell with a supersonic PD jet in a single-nozzle configuration and compare these results to previously obtained sonic PD jet data[5] in order to understand the effects of the PD jet Mach number. The results are presented in four parts. The first, second, and third sections of this paper will focus on the effects of the PD jet Mach number on the flowfield, surface, and aerodynamic properties of the aeroshell, respectively. In the last section of the paper, qualitative comparisons between numerical and experimental results will be presented to assess the validity of the computational method.

II. Technical Approach

A. Experimental Technique

Experimental results are obtained using the planar laser-induced iodine fluorescence (PLIIF) technique at a hypersonic wind tunnel facility at the University of Virginia. The PLIIF technique is a non-intrusive, spatially-resolved, time-averaged optical method for obtaining measurements in hypersonic, rarefied flows. The technique has been used for both qualitative and quantitative measurements.[6–8] PLIIF involves seeding iodine into a flowfield and exciting the molecules to a higher energy with an argon ion laser. The laser beam is turned into a thin laser sheet and passed through the flowfield of interest. The resulting fluorescence is imaged at 90 degrees using a cooled scientific-grade charge-coupled device (CCD) camera. Measurements of

the absorption spectrum are made as the laser is tuned in frequency. By fitting the measured absorption spectra at every point in the flowfield, the velocity, pressure, density, and temperature can be deduced. The technique provides qualitative flow visualization images, as well as quantitative mole fraction images, when the laser is operated in the broadband mode (laser gain profile much wider than iodine absorption linewidth). The results to be presented herein have been taken with this approach.

The hypersonic flow facility at the University of Virginia is capable of providing Mach numbers and Knudsen numbers up to 16 and 1, respectively. Hypersonic flow from an under-expanded jet is produced by the expansion of iodine-seeded nitrogen gas across a thin circular orifice of diameter $D = 2$ mm into a continuously evacuated vacuum chamber. The stagnation pressure and temperature in the wind tunnel are 1.8 atm and 300 K, respectively. Figure 1(a) presents a schematic of the experimental setup in the hypersonic flow facility. Figure 1(b) shows calculated Mach number and Knudsen number (Kn) variations inside the freejet facility.[6] These contours show the barrel shock that develops at the entrance of the test section and terminates at the Mach disk. Models are placed in the under-expanded jet core for testing at hypersonic conditions. The freestream Mach number and flow properties can be changed by adjusting the distance of the test model to the orifice.

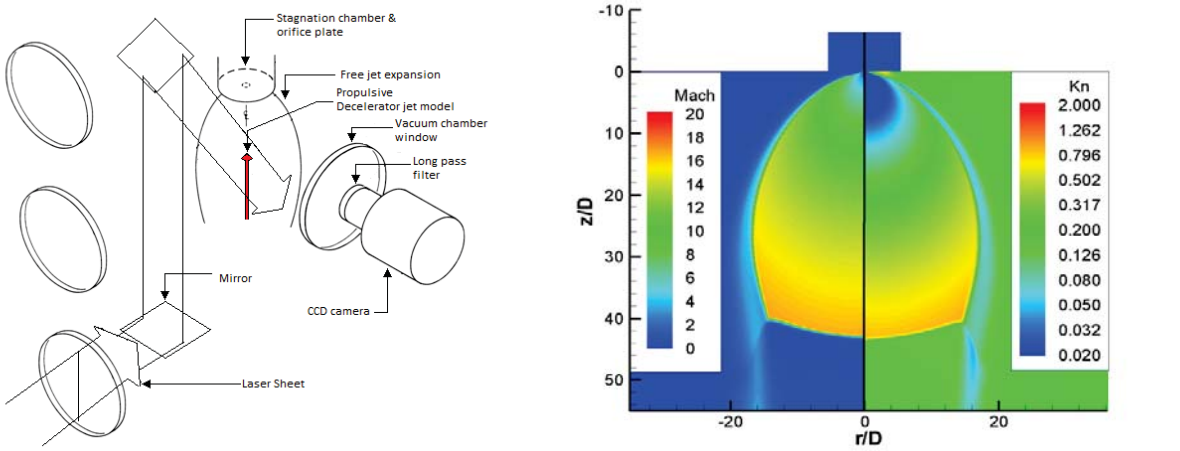

(a) Schematic of the experimental setup.

(b) Calculated Mach number and Knudsen number contours in the test section.

Figure 1. Experimental facility.

B. Numerical Method

Numerical simulations are performed using the computational fluid dynamics (CFD) code LeMANS, developed at the University of Michigan for simulating hypersonic reacting flows.[9,10] This general purpose, three-dimensional, parallel code solves the laminar Navier-Stokes equations on unstructured computational grids including thermo-chemical nonequilibrium effects with second-order spatial accuracy. The flow is modeled assuming that the continuum approximation is valid. Furthermore, for this work, it is assumed that the translational and rotational energy modes of all species can be described by two different temperatures T_{tra} and T_{rot},[11] respectively, while the vibrational energy mode and electron energy of all species are frozen at the stagnation value (i.e. 300 K). In LeMANS, the mixture transport properties can be computed using several options. In this study, Wilke's semi-empirical mixing[12] is used with species viscosities calculated using Blottner's model[13] and species thermal conductivities determined using Eucken's relation.[14]

The finite-volume method applied to unstructured grids is used to solve the set of partial differential equations. LeMANS can simulate two-dimensional and axisymmetric flows using any mixture of quadrilateral and triangular mesh cells, and three-dimensional flows using any mixture of hexahedra, tetrahedra, prisms, and pyramids. A modified Steger-Warming Flux Vector Splitting scheme is used to discretize the inviscid fluxes across cell faces, which is less dissipative and produces better results in boundary layers compared to the original scheme. The viscous terms are computed using cell-centered and nodal values. In this study,

time integration is performed using a point implicit method. LeMANS is parallelized using METIS[15] to partition the computational mesh and MPI to communicate the necessary information between processors.

III. Numerical Setup

The geometry of the aeroshell used in this study is shown in Figure 2. The aeroshell diameter is 10 mm, which is equivalent to approximately 0.22% the size of the MSL aeroshell. The PD jet is located at the center of the forebody. The PD nozzle-exit diameter is 0.9 mm and the discharge coefficient of the nozzle, defined as the ratio of actual to ideal mass flow rate, is approximately equal to 0.94.

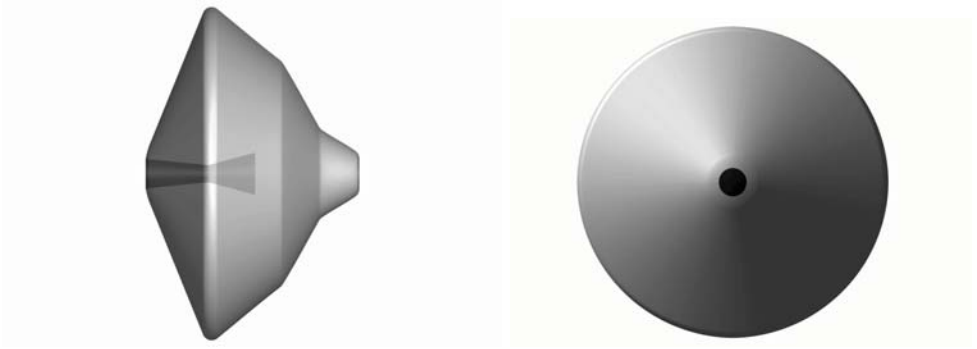

(a) Side view. (b) Front view.

Figure 2. Model geometry.

In order to accurately simulate the flow in the experimental facility, I_2-seeded N_2 gas is used in the numerical simulations with a seeding ratio of 200 ppm. The freestream rotational temperature is assumed to be equal to the translational temperature. The temperature of the aeroshell wall is assumed constant at 300 K. Radially nonuniform conditions based on the freejet relations of Ashkenas and Sherman[16] are also used as flow conditions input to LeMANS at the upstream boundary. A previous study showed that these nonuniform freestream conditions widen the bow shock around the aeroshell and decrease the drag coefficient by 6.4% compared to the uniform conditions.[17] The Mach number at a distance z away from the orifice along the centerline of the freejet is given by Eq. 1

$$M = A\left(\frac{z-z_0}{D}\right)^{\gamma-1} - \frac{1}{2}\left(\frac{\gamma+1}{\gamma-1}\right)\left[A\left(\frac{z-z_0}{D}\right)^{\gamma-1}\right]^{-1} \tag{1}$$

where D is the diameter of the freejet orifice, and A and z_0/D are constants determined for values of the ratio of specific heats γ and are equal to 3.65 and 0.40, respectively, for $\gamma = 1.4$. All other fluid properties along the freejet axis can be computed using the Mach number defined in Eq. 1, the stagnation conditions in the wind tunnel and the isentropic relations. The density distribution at a fixed distance from the orifice exit is a function of the streamline angle θ with respect to the freejet axis as shown in Eq. 2

$$\frac{\rho(\theta)}{\rho(0)} = \cos^2\left(\frac{\pi\theta}{2\Phi}\right) \tag{2}$$

where Φ is also a constant determined for each value of γ and is equal to 1.662 for $\gamma = 1.4$. For this study, a reference freestream Mach number of 12 is used in order to minimize the interaction of the bow shock around the aeroshell and the barrel shock created in the test section in the experiments. As a result, it is not necessary to model the entire test section of the wind tunnel in the numerical simulations, which dramatically cuts down on the computational cost and complexity. Figure 3, modified from McDaniel et al.,[6] shows a to-scale plot of the location of the aeroshell model with respect to the freejet orifice and velocity streamlines for the Ashkenas and Sherman boundary conditions. A set of reference freestream conditions is obtained using isentropic relations for a reference freestream Mach number of 12. These reference conditions are presented in Table 1 and are used to compute non-dimensional quantities, such as the drag coefficient. The Reynolds number based on these reference conditions and the aeroshell diameter indicates that the freestream flow is laminar.

Table 1. Reference freestream conditions.

M_{ref}	ρ_{ref} [kg/m^3]	U_{ref} [m/s]	Re_{ref}
12	4×10^{-4}	776	1100

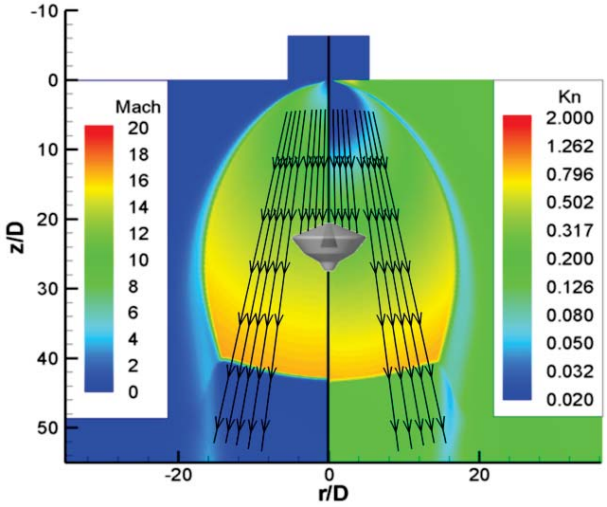

Figure 3. Ashkenas and Sherman boundary conditions and the position of the model in the test section.

The boundary conditions for the PD jet are computed such that supersonic conditions that correspond to Mach 2.66 are obtained at the nozzle-exit. These conditions are non-dimensionalized using the thrust coefficient, as defined by McGhee.[18] The thrust coefficient of a nozzle is defined as the ratio of the thrust produced by the nozzle to the product of the freestream dynamic pressure and the aeroshell frontal area. Table 2 presents the total pressure ratio, the ideal mass flow rate, and the Reynolds number based on the nozzle-exit diameter and conditions for the thrust coefficient values of interest in this study. The table also presents these conditions for the previously investigated central sonic PD jet[5] for comparison. The flow from the PD nozzle can also be assumed laminar since the jet Reynolds number for all the cases is less than 10^4.[19]

Table 2. PD jet boundary conditions.

C_T	Supersonic			Sonic		
	$P_{0,jet}/P_{0,main}$	$\dot{m}$ [kg/s]	Re	$P_{0,jet}/P_{0,main}$	$\dot{m}$ [kg/s]	Re
0.5	0.09	7.9×10^{-6}	1,000	0.11	9.1×10^{-6}	1,200
1.0	0.18	1.6×10^{-5}	2,000	0.22	1.8×10^{-5}	2,500
1.5	0.27	2.3×10^{-5}	3,100	0.33	2.8×10^{-5}	3,500
2.0	0.36	3.1×10^{-5}	4,100	0.44	3.7×10^{-5}	4,500
2.5	0.45	3.9×10^{-5}	5,100	0.55	4.6×10^{-5}	6,500

Due to the symmetry of the flowfield, axisymmetric simulations are performed using LeMANS in order to reduce the computational cost and complexity. Figure 4 shows some of the computational grids that are used in this study. These meshes are adapted by hand from previous simulations in order to align the upstream boundary of the computational domain with the bow shock. The grids are structured with quadrilateral elements because the numerical results are sensitive to the alignment of the bow shock with the grid. Cells

are clustered near the wall and in the vicinity of the PD jet in front of the aeroshell. The grid size varies from about 90,000 cells for the $C_T = 0.5$ case to approximately 110,000 cells for the $C_T = 2.5$ case. The average computational runtime for these simulations is approximately 240 CPU-hours.

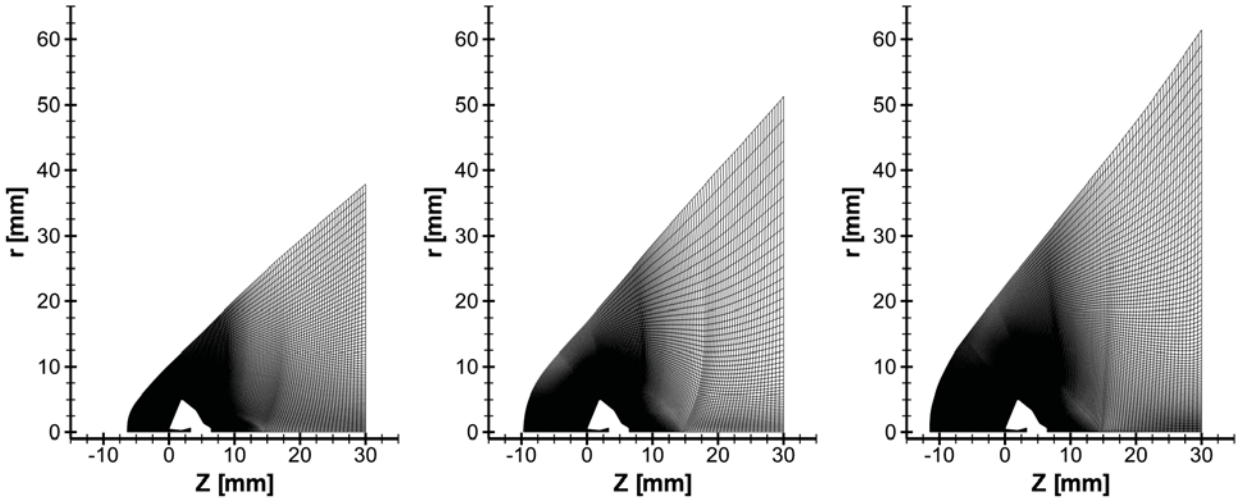

(a) $C_T = 0.5$ (b) $C_T = 1.5$ (c) $C_T = 2.5$

Figure 4. Computational grids.

IV. Results

The goal of this study is to understand the effects of the PD jet Mach number on the flowfield, surface, and aerodynamic properties of a Mars entry aeroshell using the CFD code LeMANS. The numerical results are used in qualitative comparisons with experimental data from ongoing work to assess the computational method. The surface properties are presented as non-dimensionalized pressure and skin friction coefficients defined by Eqs. 3 and 4, respectively,

$$C_P = \frac{P}{\frac{1}{2}\rho_{ref}U_{ref}^2} \tag{3}$$

$$C_f = \frac{\tau}{\frac{1}{2}\rho_{ref}U_{ref}^2} \tag{4}$$

where P is the surface pressure and τ is the wall shear stress. The drag coefficient, given in Eq. 5, is used to investigate the aerodynamic effects,

$$C_D = \frac{F_D}{\frac{1}{2}\rho_{ref}U_{ref}^2 S} \tag{5}$$

where F_D is the drag force.

A. Flowfield Effects

As mentioned in the previous section, the boundary conditions for the supersonic PD jet are computed using the isentropic relations such that the Mach number at the nozzle-exit is equal to 2.66. However, due to viscous effects in the boundary layer along the nozzle walls, the actual Mach number at the nozzle-exit is lower than 2.66. Figure 5 shows Mach number profiles along the PD jet centerline and in the nozzle-throat and nozzle-exit planes for C_T of 0.5 and 2.5. Along the jet centerline, the Mach number distribution for the two thrust coefficients are in overall close agreement with a maximum difference of 7% in the diverging section of the nozzle. Figure 5(b), however, shows that the Mach number is less than 1 at the nozzle-throat plane (approximately 0.8 for both thrust coefficients) and less than 2.66 in the nozzle-exit plane (about 2.2 and 2.3 for C_T of 0.5 and 2.5, respectively). The figure also shows that the boundary layer thickness at the nozzle-exit plane is smaller for the higher thrust coefficient case by about 50% due to the larger favorable

pressure gradient. For the remainder of this paper, the ideal 2.66 exit Mach number is used for the supersonic PD jet.

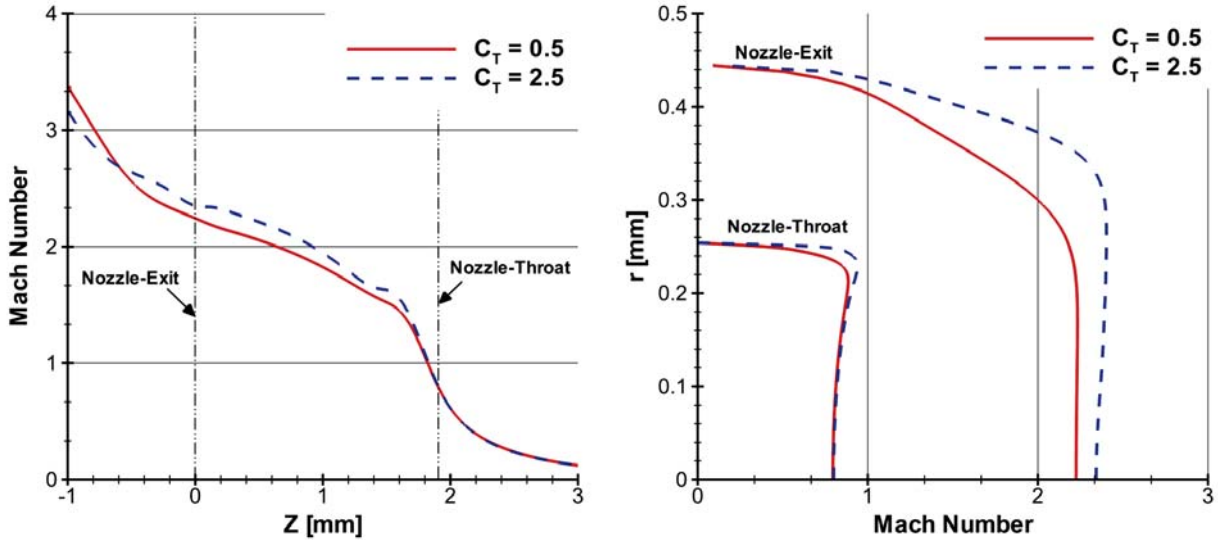

(a) Axial distribution (jet centerline)

(b) Radial distribution

Figure 5. Mach number distribution for the supersonic PD jet.

Figure 6 presents Mach number contours for supersonic (top) and sonic (bottom) central PD jets at different thrust coefficients. The figure shows that both PD jet Mach numbers generate similar flowfield features, such as PD jet shock, interface region between the bow and jet shocks that contains the detached stagnation point, and recirculation zones between the jet boundary and the aeroshell forebody. The velocity streamlines show that the apparent size of the aeroshell perceived by the freestream flow increases for both PD jet Mach numbers as the thrust coefficient increases. Several differences in these flowfield features can be observed, however, between the two PD jet Mach number cases. The figure shows that the supersonic PD jet penetrates farther upstream than the sonic jet for all thrust coefficients, which increases the standoff distances of the bow and jet shocks. The figure also shows that the width of the PD jet decreases as the Mach number increases, which is typical of supersonic jets. The recirculation zone for the supersonic PD jet is also larger than for the sonic jet. It was previously found that flow reattachment for the sonic PD jet occurs near $C_T = 2.0$.[5] Figure 6(c), however, shows that there is a separation region for the supersonic jet even at $C_T = 2.5$.

PD jet species mole fraction (i.e. tagged N_2) contours are shown in Figure 7 for supersonic (top) and sonic (bottom) PD jet at various thrust coefficients. As the thrust coefficient increases, the size of the PD jet also increases, which can be expected since the mass flow rate of the PD nozzle is proportional to the thrust force. The width of the supersonic PD jet increases from approximately an aeroshell-radius length to about 1.5 aeroshell diameters. The figure also shows that less jet species are transported downstream to the wake region by the main flow for the supersonic jet than for the sonic jet due to lower mass flow rates. Near the backshell, however, the PD jet mole fraction distribution is similar for the supersonic and sonic jets.

B. Surface Effects

The normalized pressure and shear stress along the aeroshell surface for the supersonic and sonic PD jets at thrust coefficients of 0.5, 1.5, and 2.5, as well as for the PD jet off case are presented in Figure 8. The figure shows that the overall trends for both surface pressure and shear stress are similar for the two jet Mach number cases. For pressure, first there is a decrease from the high values near the nozzle-exit as the jet expands around the sharp turning angle. This low-pressure point decreases in magnitude and moves downstream along the surface as the thrust coefficient increases. The pressure then increases to a peak near the aeroshell shoulder. The magnitude of the peak also decreases as the thrust coefficient increases. The pressure finally decreases to a roughly constant low value along the aeroshell aftbody due to the small

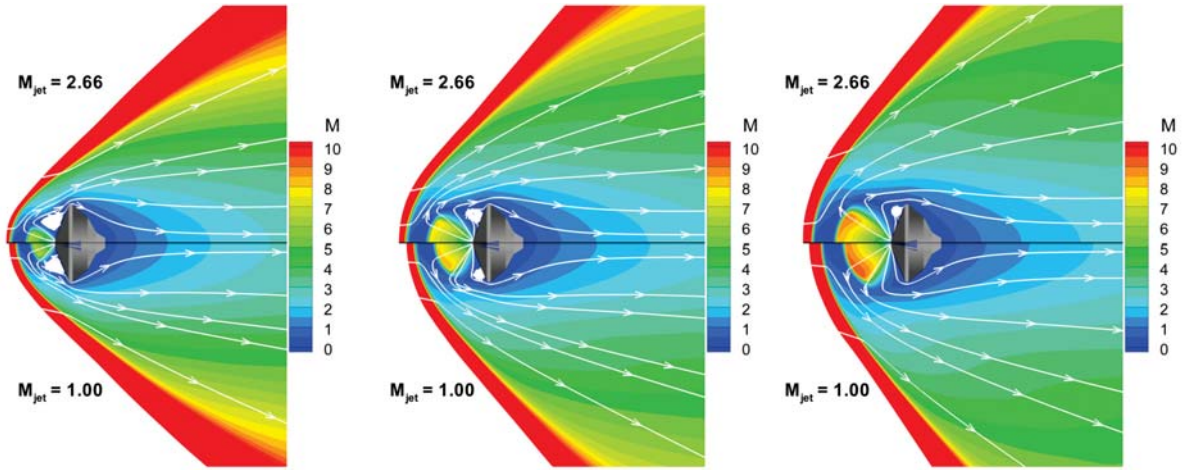

(a) $C_T = 0.5$ (b) $C_T = 1.5$ (c) $C_T = 2.5$

Figure 6. Mach number contours for supersonic (top) and sonic (bottom) central PD jet.

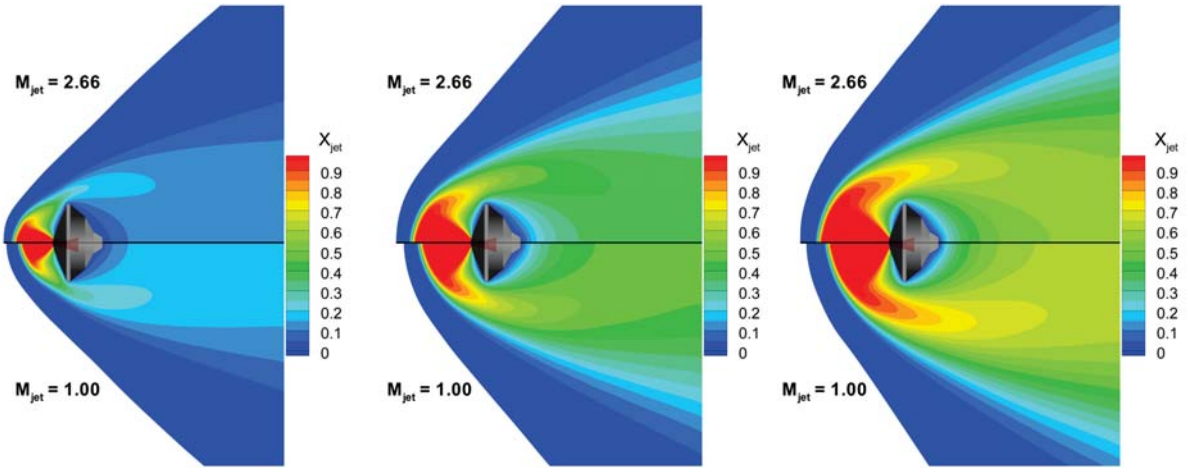

(a) $C_T = 0.5$ (b) $C_T = 1.5$ (c) $C_T = 2.5$

Figure 7. PD jet mole fraction contours for supersonic (top) and sonic (bottom) central PD jet.

velocities and densities in the wake. The wall shear stress profiles also follow a similar trend.

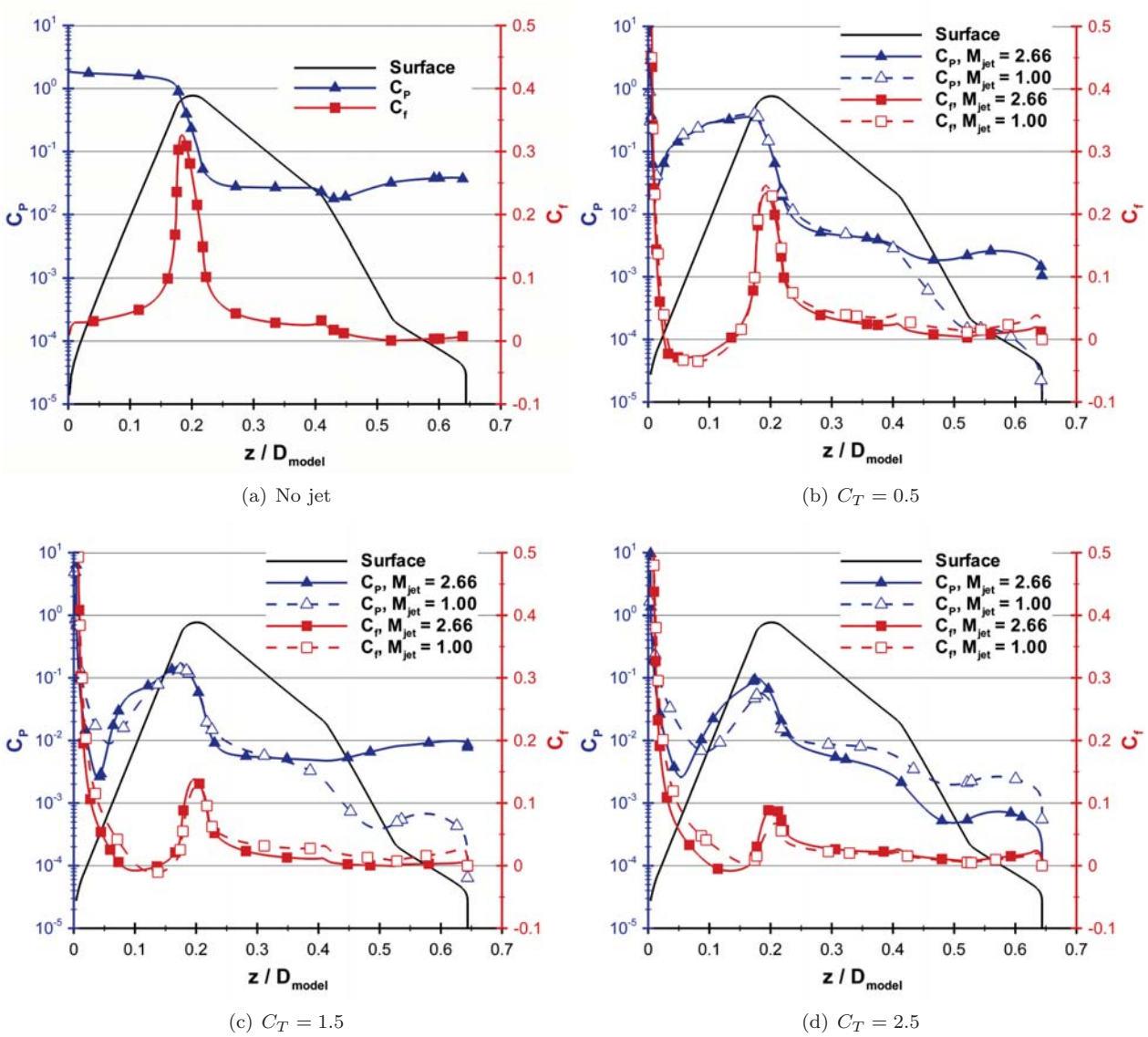

(a) No jet

(b) $C_T = 0.5$

(c) $C_T = 1.5$

(d) $C_T = 2.5$

Figure 8. Pressure and skin friction coefficient along the surface of the aeroshell for supersonic and sonic central PD jet.

Figures 8(b)-8(d), however, show some differences in the surface properties between supersonic and sonic PD jets. The surface pressure along the aftbody for the two jet Mach number cases are different. However, this variation is insignificant, especially with respect to the drag force acting on the aeroshell, due to the relatively low pressures associated with wake flows. As previously observed in the flowfield results, the supersonic PD jet generates larger recirculation regions along the aeroshell forebody (i.e. areas of negative shear-stress). This difference varies from about 3% for $C_T = 0.5$ to approximately 90% for $C_T = 1.5$ based on small regions of negative shear stress in Figure 8. For the highest thrust condition ($C_T = 2.5$), the flow is attached along the entire surface for the sonic PD jet, but there is a small recirulation region that is roughly $0.06 \times D_{model}$ long for the supersonic jet. The higher stagnation pressures and relatively lower Mach number delays the separation in the sonic PD jet cases because the flow can better overcome the sharp turning angle at the nozzle-exit. Another difference is the magnitude and location of the low-pressure point along the aeroshell forebody. The supersonic PD jet produces a low-pressure point that is smaller in magnitude and closer to the nozzle exit for all thrust coefficients compared to the sonic jet. This difference can also be attributed to the lower stagnation pressures and higher Mach number of the supersonic jet.

As discussed in a previous study,[5] the decrease in pressure and shear stress along the aeroshell surface with increasing thrust coefficient is caused by a shielding effect of the central PD jet. This shield prevents mass and momentum from reaching the surface of the aeroshell by pushing the main freestream flow upstream and creating a low pressure and shear stress region between the jet boundary and the aeroshell. Figures 9 and 10 present the mass flux (i.e. ρU) and momentum flux (i.e. $P + \rho U^2$), respectively, for the supersonic and sonic PD jets for thrust coefficients of 0.5 and 2.5. These fluxes are computed using the density of the main freestream flow (i.e. excluding the PD jet). The figures show that effects of the PD shield for the supersonic and the sonic jets are comparable. As the thrust coefficient increases, the effect of the shield also increases since less mass and momentum reach the aeroshell surface. Therefore, as the thrust coefficient increases, the flow around the aeroshell approaches a no-freestream, jet only, configuration.

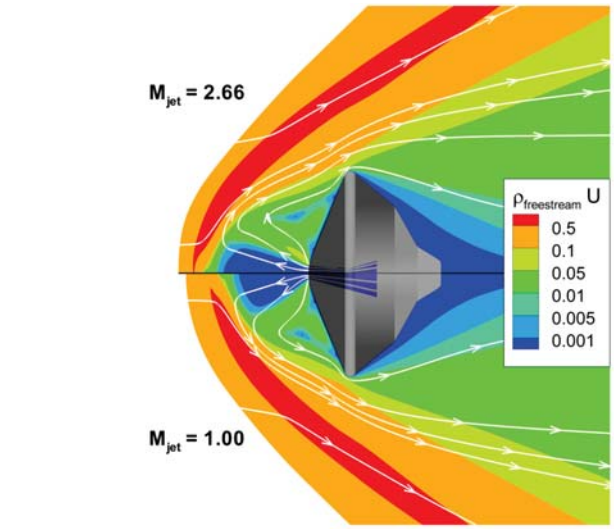

(a) $C_T = 0.5$

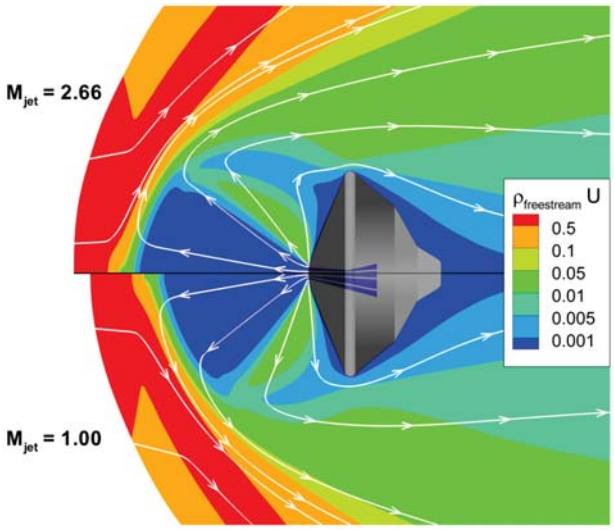

(b) $C_T = 2.5$

Figure 9. Mass transfer [kg/s·m^2]from the freestream to the surface of the aeroshell for supersonic (top) and sonic (bottom) central PD jet.

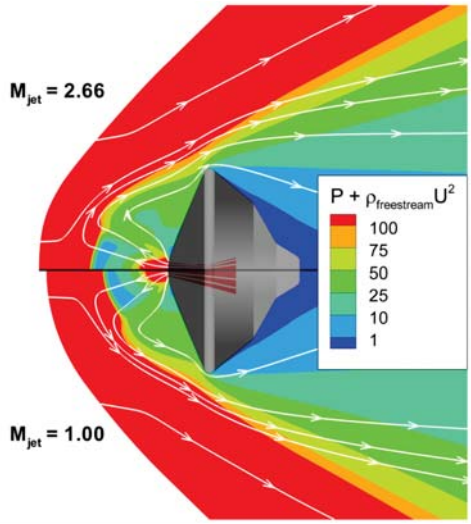

(a) $C_T = 0.5$

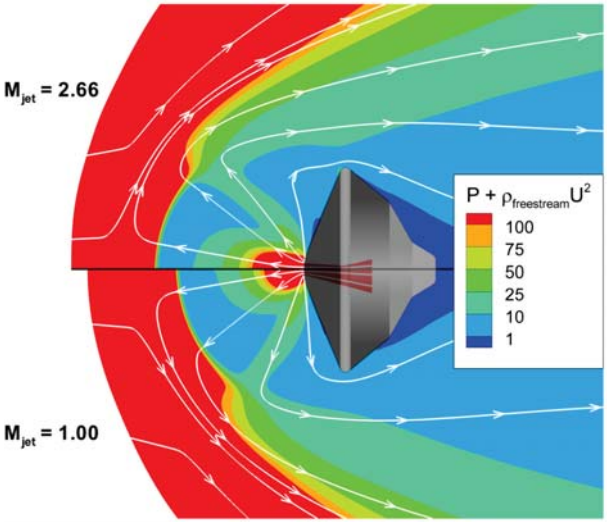

(b) $C_T = 2.5$

Figure 10. Momentum transfer [N/m^2]from the freestream to the surface of the aeroshell for supersonic (top) and sonic (bottom) central PD jet.

C. Aerodynamic Effects

The aerodynamic drag and total axial force (i.e. $C_D + C_T$) coefficients of the aeroshell for supersonic and sonic central PD jets are presented in Figure 11(a) as functions of thrust coefficient. The figure shows that the trends of the aerodynamic properties of the aeroshell for the two PD jet Mach numbers are in overall close agreement. As the thrust coefficient increases, the drag coefficient decreases and asymptotically approaches a constant value of about 6% of the no jet case for the supersonic jet. Therefore, the drag coefficient is inversely proportional to the thrust coefficient. The figure also shows that up to $C_T = 0.5$, the total axial force coefficient actually decreases as the thrust coefficient increases. For thrust coefficient values greater than 0.5, the total axial force coefficient increases due to the contribution from the PD thrust, but does not exceed the no jet value until $C_T = 1.5$ for both jet Mach numbers. Beyond $C_T = 1.5$, the total axial force coefficient increases by roughly constant increments. As previously discovered for sonic PD jets,[5] propulsive deceleration with supersonic central PD jets may also be beneficial only for relatively large thrust coefficient values that are greater than approximately 1.5. This result also appears to be independent of the jet exit Mach number, as can be seen in Figure 11(a).

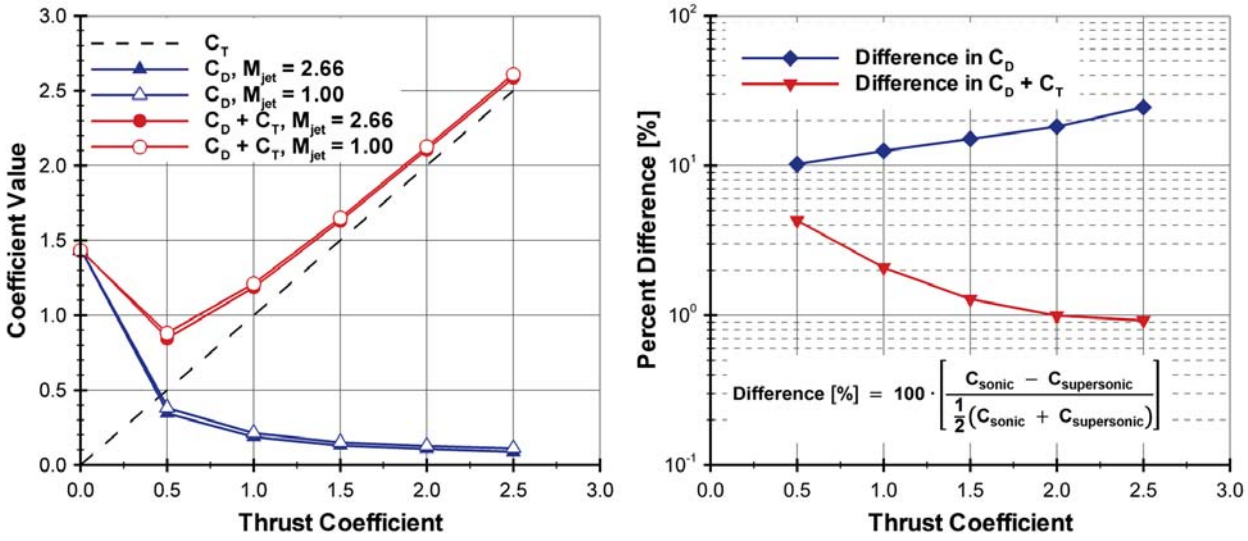

(a) Coefficient values

(b) Percent difference between supersonic and sonic PD jets

Figure 11. Comparison of drag and total axial force coefficients between supersonic and sonic PD jets.

As the thrust coefficient increases, the flow around the aeroshell approaches a jet-only, no freestream configuration due to the PD jet shield. Therefore, the effects of the PD jet Mach number on the surface properties and drag force should also increase as the thrust coefficient increases. This is shown in Figure 11(b), which shows the percent difference in drag coefficient and total axial force coefficient between the supersonic and sonic PD jets. The drag coefficient for the supersonic jet is approximately 10% and 25% lower than for the sonic jet for thrust coefficients 0.5 and 2.5, respectively. However, since the drag coefficient is inversely proportional to the thrust coefficient, the total axial force coefficient for the supersonic jet is only 4% and 1% smaller than for the sonic jet for the same thrust coefficients. This close agreement is interesting because it indicates that the jet exit Mach number does not have a significant effect on the overall deceleration performance of the aeroshell.

D. Comparison with Experimental Data

In order to assess the accuracy of the computational method, qualitative comparisons are carried out between the numerical results and experimental data obtained using the PLIIF technique. Figure 12 shows comparisons in the flowfield structure between PLIIF visualizations (images) and LeMANS (velocity streamlines) for thrust coefficients of 0.5 and 2.5. The bright areas in the PLIIF visualizations represent regions with relatively high densities. The figure shows overall good agreement in the bow shock and PD jet profiles, especially at the lower thrust coefficient. Figure 13 presents the bow shock standoff distance normalized by

the aeroshell diameter as a function of thrust coefficient for LeMANS and PLIIF. This distance is computed from the numerical results using the density field and represents the location upstream of the bow shock where the density begins to increase. The figure shows good agreement between the two techniques, with a maximum difference of about 9% for a thrust coefficient of 2.5.

(a) $C_T = 0.5$

(b) $C_T = 2.5$

Figure 12. Comparison of bow shock profile (images: PLIIF; lines: LeMANS velocity streamlines).

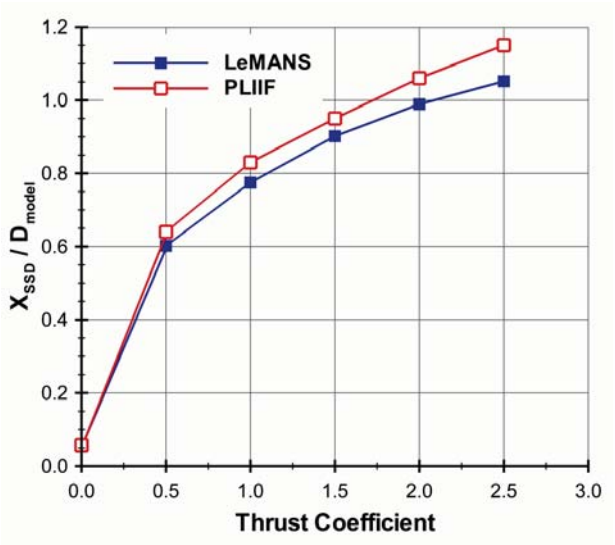

Figure 13. Comparison of bow shock standoff distance between computational and experimental data.

V. Conclusion

The effects of the PD jet Mach number on the properties of a scaled MSL aeroshell with a central jet in Mach 12 flow of I_2-seeded N_2 gas were evaluated by comparing the results for a nozzle-exit Mach number of 2.66 and previously published results for sonic jets. This was achieved using the CFD code LeMANS. In the first part of this study, the effects of the PD jet Mach number on the flowfield features were examined. The results showed that the jet Mach number approached the ideal value of 2.66 as the thrust coefficient increased due to viscous effects in the boundary layer along the nozzle walls. Similar features, such as PD jet shock and recirculation region in front of the aeroshell forebody, were observed for both the supersonic and sonic PD jets. The supersonic jet, however, was narrower and penetrated farther upstream compared to the sonic jet for all thrust coefficients. As a result, the standoff distances of the bow shock, the jet shock, and the detached stagnation point in the interface region increased. The second part of the study analyzed the effects of the PD jet Mach number on the surface properties of the aeroshell. The results showed overall similar trends between the two PD jet Mach number cases. However, there were differences in the pressure and shear stress distributions, such as the size of the recirculation region and the magnitude and location of a low-pressure point in the forebody. The third part of this study examined the PD jet Mach number effects on the aerodynamic properties. Although the trends in the drag coefficient profiles between the supersonic and sonic PD jets were similar, the difference in the values between the two jet Mach numbers increased with thrust coefficient to as much as 25% for a thrust coefficient of 2.5. The reason for this was that as the thrust coefficient increased, the flow around the aeroshell approached a jet-only, no freestream configuration due to the PD jet shield. Therefore, the effects of the PD jet Mach number on the surface properties and drag coefficient increased. However, since the drag coefficient was shown to be inversely proportional to the thrust coefficient, the total axial force coefficient for the two PD jet Mach numbers were in close agreement, with a maximum difference of 4% for a thrust coefficient of 0.5. Therefore, the PD jet Mach number was found

to have an insignificant effect on the overall deceleration performance of the aeroshell for these particular conditions. Also, propulsive deceleration with central PD jets was found to be beneficial only for relatively large thrust coefficient values that are greater than approximately 1.5 for both the sonic and supersonic jets. Finally, qualitative comparisons between the numerical and experimental results showed overall good agreement with respect to the bow shock profile and standoff distance.

VI. Future Work

For future work, the interactions of multi-nozzle PD jets will be studied in order to understand the effects of the PD jet configuration on the flowfield, surface, and aerodynamic properties of Mars entry aeroshells. The effects of continuum breakdown will also be examined using the modular particle-continuum (MPC) method, which solves the Navier-Stokes equations in regions where the continuum approximation is valid and uses the direct simulation Monte Carlo (DSMC) method in non-continuum regions. Mars entry aeroshells with PD jets in flight conditions (i.e. flight enthalpies) will be considered in order to study the effect of the PD jet heat transfer to the aeroshell.

VII. Acknowledgments

The authors gratefully acknowledge funding for this work through NASA Grant NNX08AH37A. The use of supercomputers at the University of Michigan (Center for Advanced Computing) and NASA (NASA Advanced Supercomputing Division) is essential to this work and is also greatly appreciated.

References

[1]Braun, R. D. and Manning, R. M., "Mars Exploration Entry, Descent, and Landing Challenges," *Journal of spacecraft and rockets*, Vol. 44, No. 2, March-April 2007, pp. 310–323.

[2]Edquist, K. T., Dyakonov, A. A., Wright, M. J., and Tang, C. Y., "Aerothermodynamic Environments Definition for the Mars Science Laboratory Entry Capsule," *AIAA Paper 2007-1206*, January 2007.

[3]Korzun, A. M., Braun, R. D., and Cruz, J. R., "Survey of Supersonic Retropropulsion Technology for Mars Entry, Descent, and Landing," *Journal of Spacecraft and Rockets*, Vol. 46, No. 5, September-October 2009, pp. 929–937.

[4]Dwyer-Cianciolo, A. M., Davis, J. L., Komar, D. R., Munk, M. M., Samareh, J. A., Powell, R. W., Shidner, J. D., Stanley, D. O., Wilhite, A. W., Kinney, D. J., McGuire, M. K., Arnold, J. O., Howard, A. R., Sostaric, R. R., Studak, J. W., Zumwalt, C. H., Llama, E. G., Casoliva, J., Ivanov, M. C., Clark, I., and Sengupta, A., "Entry, Descent and Landing Systems Analysis Study: Phase 1 Report," *NASA TM-2010-0000002009*, July 2010.

[5]Alkandry, H., Boyd, I. D., Reed, E. M., Codoni, J. R., and McDaniel, J. C., "Interactions of Single-Nozzle Sonic Propulsive Deceleration Jets on Mars Entry Aeroshells," *AIAA Paper 2010-4888*, June 2010.

[6]McDaniel, J. C., Glass, C. E., Staack, D., and Miller, C. G., "Experimental and Computational Comparisons of an Underexpanded Jet Flowfield," *AIAA Paper 2002-0305*, January 2002.

[7]Cecil, D. E. and McDaniel, J. C., "Planar Laser-Induced Iodine Fluorescence Measurements in Rarefied Hypersonic Flow," *Rarefied Gas Dynamics: 24th International Symposium*, Toronto, Canada, 2005, pp. 1325–1350.

[8]Reed, E. M., Codoni, J., McDaniel, J. C., Alkandry, H., and Boyd, I. D., "Investigation of the Interactions of Reaction Control Systems with Mars Science Laboratory Aeroshell," *AIAA Paper 2010-1558*, January 2010.

[9]Scalabrin, L. C. and Boyd, I. D., "Development of an Unstructured Navier-Stokes Solver for Hypersonic Nonequilibrium Aerothermodynamics," *AIAA Paper 2005-5203*, June 2005.

[10]Scalabrin, L. C. and Boyd, I. D., "Numerical Simulation of Weakly Ionized Hypersonic Flow for Reentry Configurations," *AIAA Paper 2006-3773*, June 2006.

[11]Holman, T. D. and Boyd, I. D., "Effects of Continuum Breakdown on the Surface Properties of a Hypersonic Sphere," *Journal of Thermophysics and Heat Transfer*, Vol. 23, No. 4, October-December 2009, pp. 660–673.

[12]Wilke, C. R., "A Viscosity Equation for Gas Mixtures," *Journal of Chemical Physics*, Vol. 18 No. 4, 1950, pp. 517–519.

[13]Blottner, F. G., Johnson, M., and Ellis, M., "Chemically Reacting Viscous Flow Program for Multi-Component Gas Mixtures," Tech. rep., SC-RR-70-754, Sandia Laboratories, Albuquerque, New Mexico, 1971.

[14]Vincenti, W. G. and Kruger, C. H., *Introduction to Physical Gas Dynamics*, Krieger Publishing Company, 2002.

[15]Karypis, G. and Kumar, V., "METIS: A Software Package for Partitioning Unstructured Graphs, Partitioning Meshes, and Computing Fill-Reducing Orderings of Sparse Matrices," *University of Minnesota*, 1998.

[16]Ashkenas, H. and Sherman, F. S., "The Structure and Utilization of Supersonic Free Jets in Low Density Wind Tunnels," *Contract No. NAS7-100, ONR/AFOSR Contract Review*, 1965.

[17]Alkandry, H., Boyd, I. D., Reed, E. M., and McDaniel, J. C., "Numerical Study of Hypersonic Wind Tunnel Experiments for Mars Entry Aeroshells," *AIAA Paper 2009-3918*, June 2009.

[18]McGhee, R. J., "Effects of a Retronozzle Located at the Apex of a 140 degree Blunt Cone at Mach Numbers of 3.00, 4.50, and 6.00," *NASA Technical Note D-6002*, January 1971.

[19]Pope, S. B., *Turbulent Flows*, Cambridge University Press, 2000.